

Intense high-quality medical proton beams via laser fields

Benjamin J. Galow,¹ Zoltán Harman*,^{1,2} and Christoph H. Keitel¹

¹*Max-Planck-Institut für Kernphysik, Saupfercheckweg 1, D-69029 Heidelberg, Germany*

²*ExtreMe Matter Institute EMMI, Planckstrasse 1, 64291 Darmstadt, Germany*

Abstract

During the past decade, the interaction of high-intensity lasers with solid targets has attracted much interest, regarding its potential in accelerating charged particles. In spite of tremendous progress in laser-plasma based acceleration, it is still not clear which particle beam quality will be accessible within the upcoming multi petawatt ($1 \text{ PW} = 10^{15} \text{ W}$) laser generation. Here, we show with simulations based on the coupled relativistic equations of motion that protons stemming from laser-plasma processes can be efficiently post-accelerated using crossed laser beams focused to spot radii of a few laser wavelengths. We demonstrate that the crossed beams produce monoenergetic accelerated protons with kinetic energies $> 200 \text{ MeV}$, small energy spreads ($\approx 1\%$) and high densities as required for hadron cancer therapy. To our knowledge, this is the first scheme allowing for this important application based on an all-optical set-up.

Accelerating charged particles is of paramount importance in a wide variety of fields, ranging from medicine [1–4] and material science [5] to being used to resolve the smallest structures of our universe [6, 7]. The rapid development of high-intensity laser systems which are likely to exceed in the near future $10^{25} \text{ W cm}^{-2}$ [8, 9] rendered particle beam creation by laser-matter interaction feasible. Laser-driven accelerators offer the unique feature of ultra-high electric field gradients of several TV m^{-1} , outperforming those in conventional accelerators by more than six orders of magnitude and thus offering the possibility of compact and low-cost devices [10]. Electron [11] and proton beams have recently been generated by focusing high-intensity laser light onto solid targets. This mechanism of target normal sheath acceleration (TNSA) [12–23] is realized by the strong quasi-static electric field induced by the ionization and acceleration of electrons by the intense laser field. A further laser-plasma-interaction process, the skin-layer ponderomotive acceleration (S-LPA) resulting from the huge electric potential gradient of the plasma leads to ion beams of high density [24]. To date the energy resolution and the ion kinetic energy of the generated beams merely reach the parameters required for skin-deep neoplasm, i.e. excluding deep-seated tumors. Furthermore there is still controversy [15] which beam quality, i.e. which total particle number, kinetic energy and energy spread will be accessible with the forthcoming multi petawatt-class laser systems [8, 9].

In this article we investigate the vacuum post-acceleration of plasma-generated ions by means of lasers in a single or crossed-beams configuration. This scheme of laser particle acceleration was first proposed for electrons [25–27]. The basic idea is to send the protons originating from a TNSA or S-LPA experiment through the crossing point of two laser beams at a half-angle θ with respect to the z -axis (see Fig. 1b for a scheme and a coordinate system). Within the simple plane-wave picture and assuming the laser fields to have the same amplitude, frequency, phase and to be polarized as shown in Fig. 1b, the resultant electric field component along the symmetry axis of the set-up vanishes for all points on the x -axis. At the same time, the x -component, increased by constructive interference, violently accelerates the particles. Such a coherent combination of intense beams is experimentally feasible (see p. 52 of Ref. [8]). Subsequent motion of the charged particle ejected from the focal region and no longer interacting with the laser pulse may be taken as linear. The results of our theoretical simulations demonstrate that the protons gain kinetic energies larger than 200 MeV (employing two crossed beams each with a peak intensity of $1.9 \times 10^{24} \text{ W cm}^{-2}$) with an energy spread of roughly 1%. Furthermore (assuming a realistic repetition rate of 10 Hz [8, 28]), the total number of generated protons reaches 10^{10} min^{-1} . For the first time, all

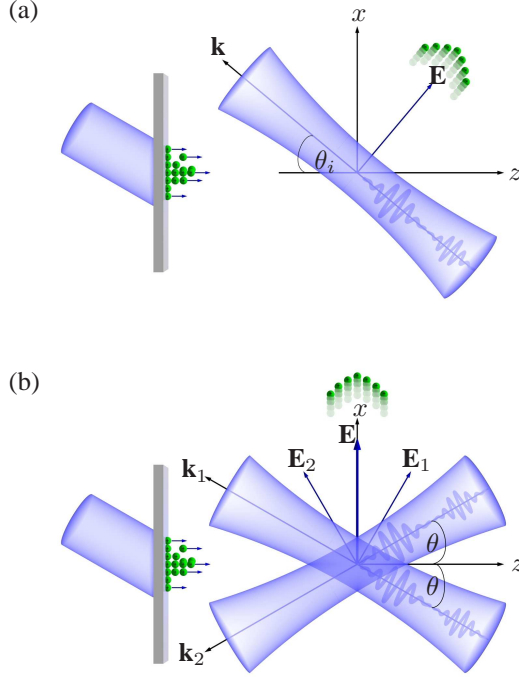


FIG. 1: Laser-proton acceleration schemes. (a) The protons, produced by laser-plasma interaction, are injected with the angle θ_i with respect to the propagation direction of a pulsed beam through its focus. The laser field polarization is denoted by \mathbf{E} and the propagation direction is given by \mathbf{k} . The protons are ejected out of the focus in the polarization direction \mathbf{E} . (b) Here, the protons are injected through the intersection point of two pulsed beams with crossing half-angle θ . The laser field polarizations are denoted by \mathbf{E}_1 and \mathbf{E}_2 and their propagation directions are given by \mathbf{k}_1 and \mathbf{k}_2 . The protons are ejected in direction of the resulting electric field \mathbf{E} .

requirements are fulfilled for broader radio-oncological use [1, 2] based on an optical accelerator.

Results

In order to generate ultra-strong accelerating fields [8, 9] of 10^{24} W cm $^{-2}$, one needs to focus the laser field to a beam waist radius on the order of the laser wavelength [29]. This necessitates an accurate description of the fields beyond the widely-used paraxial approximation. The parameters of a linearly polarized Gaussian beam which propagates in the z -direction and is polarized in the x -direction and subsequently rotated by θ_i (Fig. 1a) will be used to model the fields, i.e. the beam waist radius w_0 , the Rayleigh length $z_r = \pi w_0^2/\lambda$, where λ is the laser's wavelength, and the

diffraction angle is $\varepsilon = w_0/z_r = \lambda/(\pi w_0)$. The expressions giving the Cartesian field components $E_x, E_y, E_z, B_x, B_y, B_z$, as well as the expression for the power of the fields to order ε^{11} in the diffraction angle can be found in the Methods section and for more details we refer to Refs. [30, 31]. For the intensity profile of the employed Gaussian beams see Fig. 2.

High-intensity laser systems provide their energy in short pulses which are already sufficient to accelerate particles to high velocities [32]. Employing pulsed fields also ensures that the particles injected into the focus get captured rather than reflected. To the lowest order in time, this can be described by multiplying the electromagnetic field components with a Gaussian temporal envelope factor,

$$\begin{aligned} \mathbf{E} &\rightarrow \exp\left(-\frac{(t-z/c)^2}{2\Delta t^2}\right) \mathbf{E}, \\ \mathbf{B} &\rightarrow \exp\left(-\frac{(t-z/c)^2}{2\Delta t^2}\right) \mathbf{B}, \end{aligned} \quad (1)$$

with Δt defined via the Full Width at Half Maximum (FWHM) pulse duration $\Delta t_{\text{FWHM}} = 2\sqrt{2\log 2}\Delta t$. This approximation is valid for $T/\Delta t_{\text{FWHM}} \ll 1$, with T being the laser period. For the titanium-sapphire laser with wavelength $\lambda = 0.8 \mu\text{m}$ ($T = 2.65$ fs) and pulse durations of $\Delta t \gtrsim 10$ fs used in our simulations, this turns out to be an adequate description. Hence, further temporal corrections [33] which describe the field solutions as a dual power series in the diffraction angle ε and in the small ratio $T/(2\pi\Delta t)$ can be neglected.

The motion of an ensemble of N identical particles of mass m and charge q in the electric and magnetic fields \mathbf{E} and \mathbf{B} , respectively, of a laser beam is considered classically, with randomized initial distributions. The use of laser systems of high intensity (exceeding $10^{24} \text{ W cm}^{-2}$ for protons) requires a relativistic treatment of particle motion. Thus, the dynamics is governed by the coupled Newton-Lorentz (or energy-momentum transfer) equations (given in SI units):

$$\begin{aligned} \frac{d\mathbf{p}_j}{dt} &= q \left(\mathbf{E}(\mathbf{r}_j) + \mathbf{E}_j^{\text{int.}} + c\boldsymbol{\beta}_j \times (\mathbf{B}(\mathbf{r}_j) + \mathbf{B}_j^{\text{int.}}) \right), \\ \frac{d\mathcal{E}_j}{dt} &= qc\boldsymbol{\beta}_j \cdot (\mathbf{E}(\mathbf{r}_j) + \mathbf{E}_j^{\text{int.}}). \end{aligned} \quad (2)$$

The relativistic energy and momentum of a given particle labeled with j are denoted here by $\mathcal{E}_j = \gamma_j mc^2$ and $\mathbf{p}_j = \gamma_j mc\boldsymbol{\beta}_j$, respectively, with $\boldsymbol{\beta}_j = \mathbf{v}_j/c$ its velocity scaled by c , and $\gamma_j = (1-\beta_j^2)^{-1/2}$ its Lorentz factor. The fields mediating inter-ionic interaction are given in the Methods section. To obtain the kinetic energy gained by interaction with a laser beam, numerical solutions

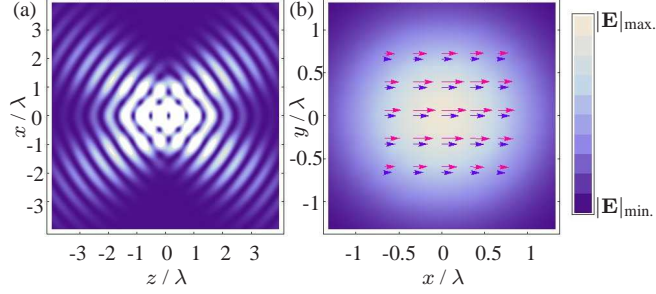


FIG. 2: Laser intensity and field strength. (a) Intensity profile of two crossed Gaussian beams in the propagation plane $y = 0$. For visualization purpose the crossing-half angle is set to $\theta = 35^\circ$. The brighter areas correspond to higher field intensity. (b) Vector field plot of the polarization plane $z = 0$ at $t = 0.2$ fs for the single beam scheme (blue arrows) with power P and crossed beam scheme (red arrows) with power $P/2$ for each beam. The constructive interference of the crossed beams results in a higher electric field strength in the intersection volume. The background of the graph shows a density map of the electric field strength $|\mathbf{E}|$ of two crossed beams in the polarization plane.

of the equations of motions will be sought. A numerical integration of equation (2) yields β_j^{fin} and, hence, γ_j^{fin} at a later final time t^{fin} taken equal to many laser field cycles. Finally, one calculates the final kinetic energy of the particle from $K_j^{\text{fin}} = \gamma_j^{\text{fin}} mc^2$.

Foremost, we carry out simulations based on the coupled equations of motion equation (2) for an ensemble of 50 particles at later used particle densities in order to determine the dominant nearest-neighbor contribution of proton-proton interaction effects on the resulting particle beam. Due to the dominating ponderomotive laser forces which lead to a fast drifting apart of the ensemble's particles, for relativistic laser intensities, i.e. $> 10^{24}$ W/cm² for protons, it turns out that the dynamics, the energy gain and its spread are influenced negligibly by inter-ionic interaction. This is in contrast to the non-relativistic laser regime. Here, the repulsive Coulomb interaction is the prevailing part of the interaction, which is in this case non-negligible compared to the electromagnetic fields of the laser. As a consequence, the accelerated ions occupy a larger phase space volume. From radio-oncological point of view we are interested in proton beams of fully relativistic energies, hence for further calculations at these energies and densities it is sufficient to study the uncoupled equations of motions only, i.e. we set $\mathbf{B}_j^{\text{int}} = \mathbf{E}_j^{\text{int}} = \mathbf{0}$ in equation (2).

The definition of a coordinate system for the crossed beams set-up depicted in Fig. 1b is given by the coordinate transformations $x_1 = x \cos \theta - z \sin \theta$, $y_1 = y$, $z_1 = x \sin \theta + z \cos \theta$ for the first beam and $x_2 = x \cos \theta + z \sin \theta$, $y_2 = y$, $z_2 = -x \sin \theta + z \cos \theta$ for the second beam, respectively.

The resulting field components which enter equation (2) are

$$\begin{aligned}
E_x &= (E_{1x} + E_{2x}) \cos \theta + (E_{1z} - E_{2z}) \sin \theta, \\
E_y &= E_{1y} + E_{2y}, \\
E_z &= (-E_{1x} + E_{2x}) \sin \theta + (E_{1z} + E_{2z}) \cos \theta, \\
B_x &= (B_{1z} - B_{2z}) \sin \theta, \\
B_y &= B_{1y} + B_{2y}, \\
B_z &= (B_{1z} + B_{2z}) \cos \theta.
\end{aligned} \tag{3}$$

Choosing a small crossing half-angle θ leads to constructive addition of the dominating x -components of the electric fields in equation (3). The adding of further laser beams would further increase the laser intensity and hence the exit kinetic energy of the accelerated particles. With respect to the energy spread one cannot achieve substantial improvement, however. For all subsequent simulations we restrict our analysis to the case of two crossed beams and set $\theta = 3^\circ$.

In order to simulate a realistic particle injection into the focal point of the laser pulses, we consider an ensemble of 5000 particles initially randomly distributed in a micron-scale volume V_{focus} oriented along the z -axis. Initially, we have to ensure that the ensemble is not already exposed to the laser fields. This is realized by starting the simulations at time $t \leq -5\Delta t$. At these initial times the electromagnetic fields are damped by the Gaussian envelope factor such that the particles' motion is only negligibly influenced by the external laser fields. Fig. 3 compares the motion of a proton starting at the same spatial point but having two different initial times. One can see

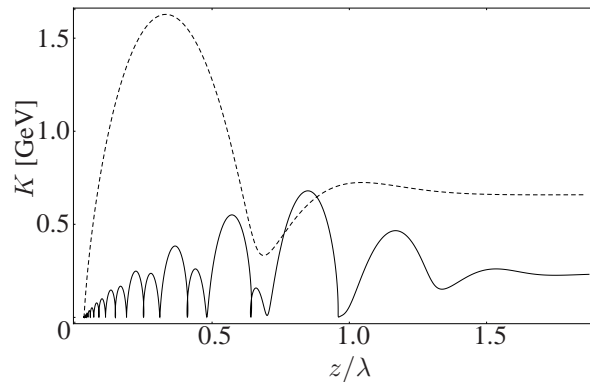


FIG. 3: Proton dynamics. Kinetic energy K for one proton initially being at rest and located at $x = z = \lambda/30$ and $y = 0$. The initial time is $t_i = 0$ (dashed line) and $t_i = -10\Delta t$ (full line). The single proton dynamics is compared at same laser parameters.

that in the unphysical case when the particle is directly exposed to the laser fields (dashed line), it immediately gains energy and is ejected out of the focus after one laser cycle. In a realistic setting, we choose an initial time of $t = -10\Delta t$: the particle slowly starts to oscillate and then gets captured and accelerated by the approaching pulse (full line). Choosing the initial time to be $t = 0$ would lead to an energy gain overestimation by a factor of approximately three.

The volume initially containing the particle ensemble has a length of the order of the laser wavelength and a radius of tens of nanometers, dependent on the focus diameter of the applied laser system, ensuring that all protons are exposed to a homogeneous field. The particles will be

TABLE I: Variation of laser parameters. Average particle kinetic energy \bar{K} and its percentual spread for different laser system parameters. $N_i = n_i \cdot V_{\text{focus}}$ is the number of ions one can accelerate as one bunch with $n_i^{\text{S-LPA}} \approx 10^{21} \text{ cm}^{-3}$ and $n_i^{\text{TNSA}} \approx 10^{19} \text{ cm}^{-3}$ is the ion density of the source used and V_{focus} denotes the volume initially containing all ions. The crossing half-angle is $\theta = 3^\circ$. The optimal particle injection angle for the single beam set-up is $\theta_i = 3^\circ$ for the S-LPA source and $\theta_i = 50^\circ$ in case of the TNSA source, respectively. For two crossed beams the particles are injected with an angle θ_c with respect to the symmetry axis (z -axis) of the laser beam configuration. In case of the S-LPA source we have $\theta_c = 0^\circ$ and for the TNSA source $\theta_c = 50^\circ$.

	\bar{K} [MeV]	N_i
S-LPA source, $P=10$ PW, $\Delta t=19.2$ fs, $w_0 = 1\lambda$		
single	28.1 ± 1.2 %	$1.0 \cdot 10^6$
crossed	59.4 ± 1.0 %	$1.0 \cdot 10^6$
S-LPA source, $P=40$ PW, $\Delta t=10.7$ fs, $w_0 = 1\lambda$		
single	113.2 ± 1.6 %	$1.0 \cdot 10^6$
crossed	233 ± 1.0 %	$1.0 \cdot 10^6$
S-LPA source, $P=100$ PW, $\Delta t=23.8$ fs, $w_0 = 2\lambda$		
single	73.2 ± 1.6 %	$1.3 \cdot 10^7$
crossed	152 ± 1.0 %	$1.3 \cdot 10^7$
TNSA source, $P=100$ PW, $\Delta t=14.4$ fs, $w_0 = 2\lambda$		
single	64.6 ± 0.7 %	$1.0 \cdot 10^5$
crossed	141 ± 0.5 %	$1.0 \cdot 10^5$

assumed to possess initial kinetic energies distributed normally around a mean value \bar{K} and having a spread ΔK . As a source we take protons originating from laser-plasma interactions, such as the S-LPA mechanism, with $\bar{K} = 17$ keV [24] and assuming a large energy spread of $\Delta K = 100\%$ or from the TNSA mechanism, with $\bar{K} = 1.2$ MeV and $\Delta K = 25\%$ [13]. The total power and the beam pulse duration are varied. Note that the peak intensity of one linearly polarized 10 PW laser beam focused to $w_0 = 1\lambda$ is already $I \sim 9.6 \times 10^{23}$ W cm⁻² [8, 9].

Discussion

Our main interest is in the energy gain, or exit kinetic energy, of the nuclei, their trajectories and, hence, the aspects that determine the quality of an accelerated beam of such nuclei. In Tab. 1, simulation results for the laser acceleration are summarized. The single and crossed beams scheme are compared at same total laser power P , pulse duration Δt and focus radius w_0 . The energy gain is ranging from 59 MeV to 233 MeV in case of the crossed beams setup and from 28 MeV to 113 MeV for injection of the ensemble into the focus of only one beam, respectively. Looking at the energy spread one can see that for the crossed beams it is always 1% and a little higher for the case of the single beam setup.

Moreover, one can see from Tab. 1 that for the systems studied here, the average exit kinetic energy \bar{K} obeys for constant injection angle and injection energy the rough scaling behavior $\bar{K} \propto I \propto P/w_0^2$. This behavior results from the fact that the optimal acceleration regime depends strongly on the pulse duration Δt rather than only on the electric field strength. It is achieved for the laser-particle interaction length being of the same order of the Rayleigh length. In Ref. [34] the same scaling behavior was derived for electrons. Therefore, in order to maximize the energy gain of the accelerated protons we first choose the laser power P and the focus radius w_0 , and then adjust to the optimal pulse duration Δt .

A further scaling law can be derived for the particle number, which is proportional to the focal volume. Using $V_{\text{focus}} \propto w_0^2 \cdot z_r$ and the definition of the Rayleigh length $z_r \propto w_0^2$, one obtains $V_{\text{focus}} \propto w_0^4$. The typical particle number needed for ion cancer treatment is 10^6 - 10^{10} per shot with a repetition rate on the order of 5 Hz [35], depending on the ionic species. For a typical interaction volume, one needs at least an ion density of $n_i = 10^6/V_{\text{focus}} \approx 10^{20}$ cm⁻³ in order to render our scheme feasible for medical applications. Using plasma-generated protons one obtains with the TNSA mechanism an ion density up to the order of $n_i^{\text{TNSA}} \approx 10^{19}$ cm⁻³ and the S-LPA ion source

generates a density of $n_i^{\text{S-LPA}} \approx 10^{21} \text{ cm}^{-3}$ [24]. The latter yields particle numbers of 10^7 per laser shot. Combined with lasers operated at 10 Hz repetition rate [8, 28] this ion number is sufficient for cancer therapy while for the TNSA mechanism a modest improvement would still be necessary.

Such improvement can e.g. be achieved by substituting the assumed titanium-sapphire laser by a super-intense CO₂ laser with a typical wave length of $\lambda = 10.6 \mu\text{m}$. Using the fact that the waist radius $w_0 \propto \lambda$ and hence the Rayleigh length $z_r \propto \lambda$, the focal region thus increases by three orders of magnitude. Consequently, the ion density needed decreases by three orders of magnitude and the needed laser intensity by two orders of magnitude. In the near future the use of high repetition rate laser systems [8, 28] will further decrease the number of protons needed per shot.

The combination of the laser-plasma mechanism as a proton source and the post acceleration process by means of single or crossed laser beams places laser acceleration of particles on the cusp of medical feasibility utilizing present-day or near-future laser technology [8, 9, 28], while anticipated costs are presently on the scale of those for current synchrotron facilities (cf. [36] and [37]). The rapid advancement of laser technology renders significant reduction likely for the near future. All requirements needed for broader radio-oncological use may be achieved: sufficient proton density and exit kinetic energies, and sharp energy spread of approximately 1 %. The scheme that we introduce in the present work calls for tight focusing mechanisms [29] and relies on results of laser-plasma-interaction research [12–23].

Methods

Description of a tightly focused linearly polarized beam

The electromagnetic field components of the tightly focused linearly polarized beams which we employ in our simulations can be given as a power series in the diffraction angle ε . Their functional

form is given by

$$\begin{aligned}
E_x &= E \left\{ S_1 + \varepsilon^2 \left[\xi^2 S_3 - \frac{\rho^4 S_4}{4} \right] + \dots + \mathcal{O}(\varepsilon^{10}) \right\}, \\
E_y &= E \xi v \left\{ \varepsilon^2 [S_3] + \dots + \mathcal{O}(\varepsilon^{10}) \right\}, \\
E_z &= E \xi \left\{ \varepsilon [C_2] + \dots + \mathcal{O}(\varepsilon^{11}) \right\}, \\
B_x &= 0, \\
B_y &= \frac{E}{c} \left\{ S_1 + \varepsilon^2 \left[\frac{\rho^2 S_3}{2} - \frac{\rho^4 S_4}{4} \right] + \dots + \mathcal{O}(\varepsilon^{10}) \right\}, \\
B_z &= \frac{E}{c} v \left\{ \varepsilon [C_2] + \dots + \mathcal{O}(\varepsilon^{11}) \right\}.
\end{aligned} \tag{4}$$

With ω the angular frequency of the fields, $\xi = x/w_0$, $v = y/w_0$, $\zeta = z/z_r$, $\psi_G = \tan^{-1} \zeta$, and $r = \sqrt{x^2 + y^2}$, $\rho = r/w_0$, the remaining symbols in equation (4) have the following definitions

$$\begin{aligned}
E &= E_0 e^{-r^2/w^2}; \quad w = w_0 \sqrt{1 + \zeta^2}, \\
C_n &= \left(\frac{w_0}{w} \right)^n \cos(\psi + n\psi_G); \quad n = 1, 2, 3, \dots, \\
S_n &= \left(\frac{w_0}{w} \right)^n \sin(\psi + n\psi_G),
\end{aligned} \tag{5}$$

where

$$\psi = \psi_0 + \omega t - kz - \frac{kr^2}{2R}; \quad R = z + \frac{z_r^2}{z}, \tag{6}$$

and ψ_0 is a constant initial phase. Also, t is the time and $k = 2\pi/\lambda$ is the wavenumber. On the other hand, with $E_0 \rightarrow E_{0l}$, the power expression may be given, to the same order in ε as the field components, by

$$\begin{aligned}
P_l &= \frac{\pi w_0^2 E_{0l}^2}{4 c \mu_0} \left[1 + \left(\frac{\varepsilon}{2} \right)^2 + 2 \left(\frac{\varepsilon}{2} \right)^4 + 6 \left(\frac{\varepsilon}{2} \right)^6 \right. \\
&\quad \left. + \frac{45}{2} \left(\frac{\varepsilon}{2} \right)^8 + \frac{195}{2} \left(\frac{\varepsilon}{2} \right)^{10} \right],
\end{aligned} \tag{7}$$

where c is the speed of light in vacuum, μ_0 is the permeability of free space and E_{0l} is the electric field amplitude, with l standing for linearly polarized. Note that $E_{0l} \propto \sqrt{P_l}$ and that the leading term in E_{0l} is inversely proportional to w_0 . For more details we refer to Refs. [30, 31].

Relativistic coupled equations of motion

The fields mediating the inter-ionic interaction in the relativistic coupled equations of motion

(2) are modeled by $\mathbf{E}_j^{\text{int}} = \sum_{k \neq j} (-\nabla \phi_{jk} - \frac{\partial}{\partial t} \mathbf{A}_{jk})$ and $\mathbf{B}_j^{\text{int}} = \sum_{k \neq j} (\nabla \times \mathbf{A}_{jk})$ with $j, k \in \{1, 2, \dots, N\}$. The interaction potentials read

$$\phi_{jk} = \frac{q}{4\pi\epsilon_0} \frac{1}{|\mathbf{r}_j - \mathbf{r}_k|}, \quad (8)$$

$$\mathbf{A}_{jk} = \frac{q}{8\pi\epsilon_0 c^2 |\mathbf{r}_{jk}|} \left(\mathbf{v}_k + \frac{\mathbf{r}_{jk}(\mathbf{v}_k \cdot \mathbf{r}_{jk})}{|\mathbf{r}_{jk}|} \right), \quad (9)$$

with the relative displacement $\mathbf{r}_{jk} = \mathbf{r}_j - \mathbf{r}_k$ and ϵ_0 being the vacuum permittivity. Equation (8) is the scalar part of the interaction given by the Coulomb potential, whereas relativistic effects such as retardation and current-current interaction are included in the Darwin vector potential up to $\mathcal{O}(\beta^2)$ [38] in equation (9). Typical kinetic energies of the accelerated protons are of about 200 MeV (cf. Tab. 1), which corresponds to $\beta^2 \approx 0.3$. Consequently, the truncation of the interaction up to $\mathcal{O}(\beta^2)$ is justified and higher-order contributions such as those up to $\mathcal{O}(\beta^4)$ in Ref. [39] will not be taken into account.

Equation (2) is a differential algebraic equation of the form

$$\begin{aligned} \frac{d\boldsymbol{\beta}_1}{dt} &= f_1 \left(\mathbf{r}_1, \dots, \mathbf{r}_N, \boldsymbol{\beta}_1, \dots, \boldsymbol{\beta}_N, \frac{d\boldsymbol{\beta}_1}{dt}, \dots, \frac{d\boldsymbol{\beta}_N}{dt}, t \right), \\ &\vdots \\ \frac{d\boldsymbol{\beta}_N}{dt} &= f_N \left(\mathbf{r}_1, \dots, \mathbf{r}_N, \boldsymbol{\beta}_1, \dots, \boldsymbol{\beta}_N, \frac{d\boldsymbol{\beta}_1}{dt}, \dots, \frac{d\boldsymbol{\beta}_N}{dt}, t \right). \end{aligned} \quad (10)$$

For each time step the system has to be solved algebraically with respect to $\frac{d\boldsymbol{\beta}_1}{dt}, \dots, \frac{d\boldsymbol{\beta}_N}{dt}$. Then, a standard fourth-order Runge-Kutta algorithm is used to integrate the remaining system of ordinary differential equations.

Acknowledgments

ZH acknowledges conversations with Y. I. Salamin. Supported by Helmholtz Alliance HA216/EMMI.

-
- [1] Yock, T. I. & Tarbell, N. J. Technology Insight: proton beam radiotherapy for treatment in pediatric brain tumors. *Nature Clinical Practice Oncology* **1**, 97–103 (2004).
- [2] Levin, M. P., Kooy, H., Loeffler, J. S. & DeLaney, T. F. Proton beam therapy. *British Journal of Cancer* **93**, 849–854 (2005).

- [3] Jäkel, O., Krämer, M., Karger, C. P. & Debus, J. Treatment planning for heavy ion radiotherapy: clinical implementation and application. *Phys. Med. Biol.* **46**, 1101–1116 (2001).
- [4] Combs, S. E. *et al.* Carbon ion radiotherapy for pediatric patients and young adults treated for tumors of the skull base. *Cancer* **115**, 1348–1355 (2009).
- [5] van Kan, J. A., Bettioli, A. A. & Watt, F. Three-dimensional nanolithography using proton beam writing. *Appl. Phys. Lett.* **83**, 1629–1631 (2003).
- [6] Ledingham, K. W. D., McKenna, P. & Singhal, R. P. Applications for nuclear phenomena generated by ultra-intense lasers. *Science* **300**, 1107–1111 (2003).
- [7] LHC–The Large Hadron Collider. <http://lhc.web.cern.ch/lhc/>.
- [8] The Extreme Light Infrastructure European Project (ELI). Scientific Case (2007). <http://www.extreme-light-infrastructure.eu/pictures/ELI-scientific-case-id17.pdf>.
- [9] High Power Laser Energy Research (HiPER). HiPER technical background and conceptual design report. <http://www.hiperlaser.org/docs/tdr/HiPERTDR2.pdf>.
- [10] Dunne, M. Laser-driven particle accelerators. *Science* **312**, 374–376 (2006).
- [11] Malka, V. *et al.* Electron acceleration by a wake field forced by an intense ultrashort laser pulse. *Science* **298**, 1596–1600 (2002).
- [12] Hegelich, B. M. *et al.* Laser acceleration of quasi-monoenergetic MeV ion beams. *Nature* **439**, 441–444 (2006).
- [13] Schwoerer, H. *et al.* Laser-plasma acceleration of quasi-monoenergetic protons from microstructured targets. *Nature* **439**, 445–448 (2006).
- [14] Fuchs, J. *et al.* Laser-driven proton scaling laws and new paths towards energy increase. *Nature Physics* **2**, 48–54 (2006).
- [15] Robson, L. *et al.* Scaling of proton acceleration driven by petawatt-laser-plasma interactions. *Nature Physics* **3**, 58–62 (2007).
- [16] Maksimchuk, A., Gu, S., Flippo, K., Umstadter, D. & Bychenkov, V. Y. Forward ion acceleration in thin films driven by a high-intensity laser. *Phys. Rev. Lett.* **84**, 4108–4111 (2000).
- [17] Snavely, R. A. *et al.* Intense high-energy proton beams from petawatt-laser irradiation of solids. *Phys. Rev. Lett.* **85**, 2945–2948 (2000).
- [18] Karsch, S. *et al.* High-intensity laser induced ion acceleration from heavy-water droplets. *Phys. Rev. Lett.* **91**, 015001 (2003).
- [19] Romagnani, L. *et al.* Dynamics of electric fields driving the laser acceleration of multi-MeV protons.

- Phys. Rev. Lett.* **95**, 195001 (2005).
- [20] Cowan, T. E. *et al.* Ultra-low emittance, high current proton beams produced with a laser-virtual cathode sheath accelerator. *Nucl. Instr. Meth. Phys. Res.* **544**, 277–284 (2005).
- [21] Albright, B. J. *et al.* Theory of laser acceleration of light-ion beams from interaction of ultrahigh-intensity lasers with layered targets. *Phys. Rev. Lett.* **97**, 115002 (2006).
- [22] Tajima, T. & Dawson, J. M. Laser electron accelerator. *Phys. Rev. Lett.* **43**, 267–270 (1979).
- [23] Mackinnon, A. J. *et al.* Effect of plasma scale length on multi-MeV proton production by intense laser pulses. *Phys. Rev. Lett.* **86**, 1769–1772 (2001).
- [24] Badziak, J. Laser-driven generation of fast particles. *Opto-Electr. Review* **15**, 1–12 (2007).
- [25] Haaland, C. M. Laser electron acceleration in vacuum. *Opt. Commun.* **114**, 280–284 (1995).
- [26] Esarey, E., Sprangle, P. & Krall, J. Laser acceleration of electrons in vacuum. *Phys. Rev. E* **52**, 5443–5453 (1995).
- [27] Salamin, Y. I., Keitel, C. H. Subcycle high electron acceleration by crossed laser beams. *Appl. Phys. Lett.* **77**, 1082–1084 (2000).
- [28] Major, Z. *et al.* Basic concepts and current status of the petawatt field synthesizer – a new approach to ultrahigh field generation. *The Review of Laser Engineering* **37**, 431–436 (2009).
- [29] Bahk, S.-W. *et al.* *Opt. Lett.* **29**, 2837–2839 (2004).
- [30] Salamin, Y. I. Fields of a Gaussian beam beyond paraxial approximation. *Appl. Phys. B* **86**, 319–326 (2007).
- [31] Salamin, Y. I., Harman, Z. & Keitel, C. H. Direct high-power laser acceleration of ions for medical applications. *Phys. Rev. Lett.* **100**, 155004 (2008).
- [32] Wang, J. X. *et al.* High-intensity laser-induced electron acceleration in vacuum. *Phys. Rev. E* **60**, 7473–7478 (1999).
- [33] Yan, Z. *et al.* Accurate description of ultra-short tightly focused Gaussian laser pulses and vacuum laser acceleration. *Appl. Phys. B* **81**, 813–819 (2005).
- [34] Stupakov, G. V. & Zolotarev, M. S. Ponderomotive laser acceleration and focusing in vacuum for generation of attosecond electron bunches. *Phys. Rev. Lett.* **86**, 5274–5277 (2001).
- [35] Eickhoff, H. *et al.* HIT–Heidelberg Ion beam Therapy. Scientific Case. http://www-aix.gsi.de/~spiller/facilit_ep00.ps.
- [36] HIT–Heidelberg Ion beam Therapy. Facts in short. <http://www.klinikum.uni-heidelberg.de/HIT-Fac>
- [37] Gerstner, E. Laser physics: extreme light. *Nature* **446**, 16–18 (2007).

- [38] Jackson, J. D. *Classical Electrodynamics* (John Wiley & Sons, 1999), third edn.
- [39] Jaén, X., Llosa, J. & Molina, A. A reduction of order two for infinite-order Lagrangians. *Phys. Rev. D* **34**, 2302–2311 (1986).